International Journal of Microwave and Wireless Technologies

cambridge.org/mrf

Pattern diversity and isolation enhancement of UWB MIMO antenna based on characteristic modes for mobile terminals

Shailesh Jayant[1,2], Garima Srivastava[3] and Sachin Kumar[4]

[1]Guru Gobind Singh Indraprastha University, Delhi, 110078, India; [2]Department of Electronics and Communication Engineering, Ambedkar Institute of Advanced Communication Technologies and Research, Geeta Colony, Delhi, 110031, India; [3]Department of Electronics and Communication Engineering, Netaji Subhas University of Technology, Geeta Colony, Delhi, 110031, India and [4]Department of Electronics & Communication Engineering, SRM Institute of Science and Technology, Chennai, 603203, India

Research Paper

Cite this article: Jayant S, Srivastava G, Kumar S (2023). Pattern diversity and isolation enhancement of UWB MIMO antenna based on characteristic modes for mobile terminals. *International Journal of Microwave and Wireless Technologies* **15**, 793–804. https://doi.org/10.1017/S1759078722000757

Received: 23 December 2021
Revised: 7 June 2022
Accepted: 7 June 2022

Key words:
UWB; MIMO; ECC; Characteristic Modes; Vivaldi Antenna

Author for correspondence:
Garima Srivastava;,
E-mail: garima.shrivastav@gmail.com

Abstract

A printed ultra-wideband (UWB) multiple input multiple output antenna with isolation enhancement and pattern diversity is presented, which is based on characteristic modes (CM) for upcoming wireless mobile platforms. The presented antenna is composed of dual UWB antenna elements (AEs) – an antipodal Vivaldi and a circular-shaped monopole positioned on the two opposite edges of the antenna's rectangular-shaped ground surface. The two AEs are capable to stimulate distinct modes in the ground surface and therefore obtaining the required distinct radiation (far-field) patterns and highly isolated AEs without introducing any decoupling structure (DS). The measured results demonstrate that both AEs are UWB with an operating frequency from 2.6 to 11 GHz. The measured isolation is more than 30.1 dB with a maximum value of 55 dB in UWB. The peak realized gain is over 0.83 dBi. The radiation efficiency is greater than 75%. The Envelope Correlation Coefficient is <0.08.

Introduction

The future mobile access technology needs high spectral efficiency and wide channel capacity [1–3], which can be fulfilled by incorporating wide bandwidth and MIMO technology in 5 G mobile terminals. Therefore, an ultra-wideband (UWB) multiple input multiple output (MIMO) antenna is designed for mobile devices. In MIMO antennas, pattern diversity is utilized to exploit multipath fading. Pattern diversity comprises at least two neighboring antennas with various radiation patterns. This diversity utilizes directional antennas, which are generally physically isolated by a short gap [4]. Antennas with various radiation patterns are utilized in the pattern diversity strategy. These two distinct kinds of antennas will encounter uncorrelated fading and henceforth this diversity idea is taken advantage of to recuperate the communicated data at receiving end. To accomplish great performance under this plan, antennas should be set nearer. For instance, cell phones have double antennas such as microstrip and dipole antennas [5]. Pattern diversity further develops the unwavering quality of a message signal by utilizing at least two communication channels with various attributes. The pattern diversity likewise assumes an indispensable part in removing fading, co-channel interference, and keeping away from error bursts [6].

In the last few years, the MIMO antenna is designed with different AE arrangements such as orthogonal, parallel, 180° rotation, etc. to enhance isolation. To further increase the isolation, in each arrangement, different types of decoupling techniques (DT) are used as shown in Table 1 such as parasitic element, orthogonal position, 180° rotation, decoupling structure (DS), defected ground structure (DGS), metamaterial, neutralization line (NL) and carbon black film, etc. The description, limitation, and highest isolation of each DT are also mentioned in Table 1. Based on Table 1, it is clear that each DT has its limitation/s and the highest isolation provided by these DTs is 25 dB. However, for applications such as mobile terminals and future wireless communications, there is a need for isolation of more than 25 dB.

As of late, the new concept of utilizing the CM for exciting distinct modes has been proposed to achieve distinct radiation patterns and high isolation in MIMO antenna with no extra DS [22–24]. This new strategy can be stretched out to construct a UWB MIMO antenna. It has been suggested that the same CM is not shared by the two AEs at two edges of the ground surface [22]. Because the two AEs do not share the same CM on the ground surface, they are isolated easily with distinct patterns and low mutual coupling. But, a mobile antenna requires excitation of the ground surface successfully for optimizing

© The Author(s), 2022. Published by Cambridge University Press in association with the European Microwave Association

Table 1. Different types of decoupling techniques

DT	Description	Limitation	Highest isolation (dB)
Parasitic element [7]	Conducting structure is placed between antenna elements, which act as a reflector and is not connected to ground	There is no common ground, which is required to have the same voltage level and preferred for the practical purpose	25
Orthogonal position [8]	Antenna elements are positioned orthogonally	Unable to suppress coupling effect in the lower frequency as compared to the higher frequency	20.6
180° Rotation [9, 10]	Antenna elements are positioned at 180° concerning each other	Does not improve the isolation and pattern diversity so much.	20.2
Decoupling structure [9, 11–16]	Conducting structure attached to the ground	High level of cross-polarized radiation patterns	21
Defected ground structure [17, 18]	Introducing various slits/slots in the ground surface is usually utilized profiting from the mix of capacitance and inductance	Slits/slots in the ground surface are not preferable for housing and increasing fabrication complexity	25
Metamaterial [19]	Metamaterial is organized between dual electromagnetically coupled patches to remove the surface wave coupling	It makes the system complex	16
Neutralization line [20]	Conducting structure connected to the feeding lines	Occupies additional space and is suitable for narrowband operation	22
Carbon black film [21]	Absorbs the interference between two or more antenna elements	Distort the radiation patterns	15

the performance of the antenna. The above-mentioned design concept for the MIMO antenna can be improved by designing the two AEs for stimulating distinct CM on the ground surface. Furthermore, in place of half-loop AE, antipodal Vivaldi AE (AE1) is used. Additionally, circular monopole AE is also utilized (AE2). Both AEs are wideband antennas and useful for obtaining the UWB frequency range.

This research paper presented a printed UWB MIMO mobile antenna explained with the help of CM. The dual distinct AEs are kept on the opposite edges of the antenna's rectangular-shaped ground surface. The two AEs have dissimilar current distributions, which results in the excitation of dissimilar CM. The two AEs refer to as magnetic and electric sources. Thus exciting two orthogonal CM. The distinct CM can produce the required isolation and distinct radiation patterns. Like this, the same concept of CM has been used in the presented UWB MIMO antenna. The tested results verify that the presented technique operates well for the UWB MIMO mobile antenna.

Construction of presented antenna

The MIMO antenna is designed by placing the ground surfaces of two AEs (AE 1 and AE 2) at the opposite edges of the rectangular structure of size $10 \times 42\ mm^2$ [25]. The AE1 is the antipodal Vivaldi antenna and AE 2 is the circular monopole antenna. The complete simulated and fabricated structures of the designed antenna are displayed in Figs 1(a) and 1(b), respectively. The MIMO antenna is designed on an FR4 dielectric substrate with a dielectric constant of 4.4, the height of substrate of 1.4 mm, and a loss tangent of 0.02. The complete chip size of the presented MIMO antenna is $100.16 \times 42\ mm^2$.

The individual design of AEs are displayed in Figs 2(a) and 2(b), respectively with the S_{ii} plot in Fig. 2(c). Additionally, the

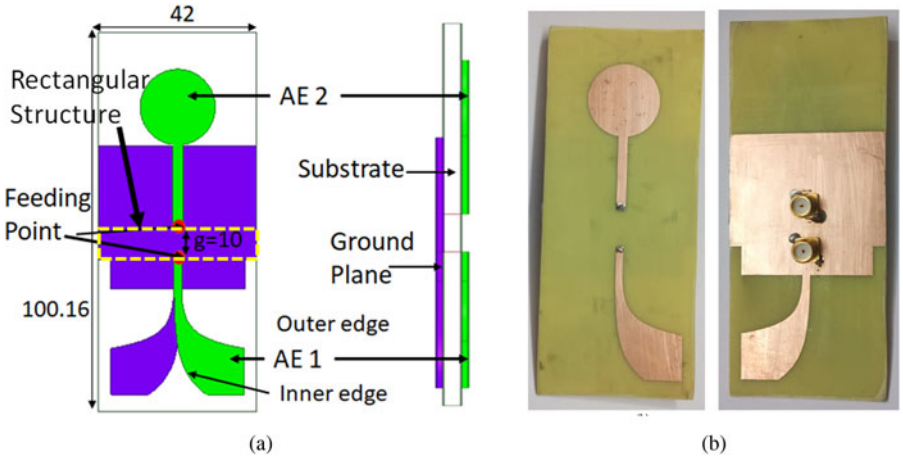


Fig. 1. (a) Structure and dimensions (in mm) of the presented antenna and (b) fabricated antenna with front and back view.

https://doi.org/10.1017/S1759078722000757 Published online by Cambridge University Press

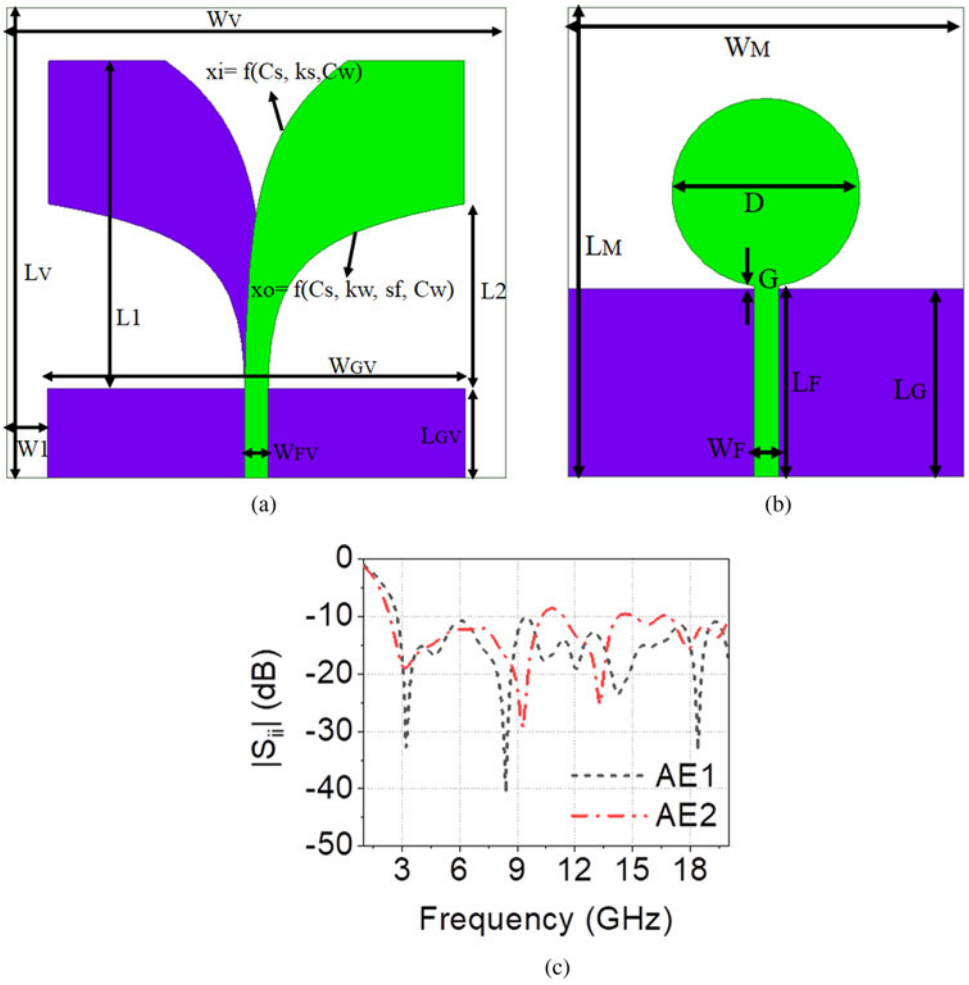


Fig. 2. Structure of (a) Antipodal Vivaldi antenna (AE1), (b) Circular monopole antenna (AE2), and (c) S_{11} of AE1 and AE2.

dimensions of all the variables of both AEs are shown in Table 2. In the AE1, dual exponentially tapered symmetric patches are designed on the back and front sides of the substrate with microstrip transmission line feeding. The inner and outer edge tapers of the AE1 are referred as

$$x_i = \pm C_s.exp(k_s y) \mp (C_s + 0.5C_w) \quad (1)$$

$$x_o = \pm C_w.exp(k_w y^{sf}) \mp (C_s + 0.5C_w) \quad (2)$$

where x_o and x_i represent the gaps from the slot centerline to the outer and inner edges, respectively [26]. The C_s determine slot width at the feeding interface and k_s determine the rate by which the slot opens. The x_o is the function of coefficients of outer edge taper such as C_w, k_w, and sf. The design equation of AE1 is shown below equation (3):

$$f_{rL}(GHz) = \frac{c}{2\,L1\sqrt{\frac{\varepsilon_r + 1}{2}}} \quad (3)$$

here, f_{rL} is a lower resonance frequency in (GHz). When the value of L1 in mm and ε_r are put in equation (3), $f_{rL} = 3.26$ GHz (calculated), which is almost matched with the simulated value (3.2 GHz).

In AE2, a circular monopole antenna with microstrip line feeding is designed on the front side of the substrate. The design equation of AE2 is given by the following equation [27]:

$$f_{rL}\ (\text{GHz}) = \frac{14.4}{L_G + D + G + (1/2\pi\sqrt{\varepsilon_r})((A_G/L_G) + (A_P/D))} \quad (4)$$

where, L_G = Length of the ground surface, D = Diameter of the circle, G = Distance between patch and ground surface, A_G = Area of the ground plane, A_P = Area of the circular patch, and ε_r = Dielectric constant of the substrate. Note that all dimensions of AE2 are in cm for calculating f_{rL} in (GHz). By putting the values of the variable in the formula (4), $f_{rL} = 3.212$ GHz (calculated), which is almost equal to the simulated value of 3.2 GHz.

As presented in Fig. 3, three cases of the presented antenna are compared. In the first case, both antenna elements are antipodal Vivaldi antennas and in the second case, both antenna elements are circular monopole antennas, and the third case is proposed MIMO antenna with AE1 and AE2, which are oriented in 180° direction with a spacing of 10 mm. It is concluded that in all

https://doi.org/10.1017/S1759078722000757 Published online by Cambridge University Press

Table 2. Values of the various parameters of AE1 and AE2

Antipodal Vivaldi antenna (AE1)				Circular monopole antenna (AE2)	
Parameter	Value (in mm)	Parameter	Value (in mm)	Parameter	Value (in mm)
Cs	0.1	LGV	7.6	L_M	50
Cw	1.5	WGV	35.56	W_M	42
Ks	0.16	L1	28	L_F	20.3
Kw	0.01	L2	15.8	W_F	2.6
Sf	2	W1	3.5	L_G	20
LV	40.16	WFV	2	D	20
WV	42.56			G	0.3

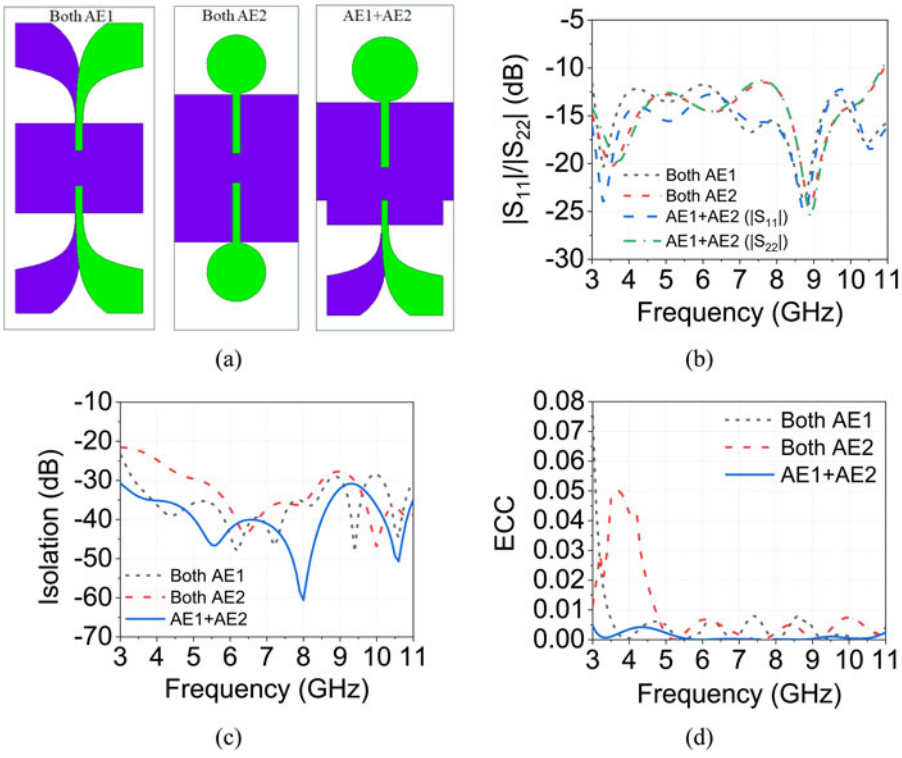


Fig. 3. (a) Structure of three cases of MIMO antenna, (b) S_{ii}, (c) Isolation, and (d) ECC.

cases UWB bandwidth is achieved with better impedance matching and isolation of the proposed MIMO antenna higher than in the other two cases as presented in Table 3. Also, the peak value of ECC is the lowest in the proposed MIMO antenna case (Table 3).

Figure 4(a) displays the equivalent circuit model of the presented AEs and MIMO antenna. This circuit is designed by examining the *s*-parameter S_{ii} of the antenna using the circuit simulator of HFSS. By attaining the s-parameter, the overall circuit has been changed to indicate the properties of the antenna. The patch is represented by a parallel RLC circuit and the probe inductance is represented by a series inductor. The presented antenna is lossy because of the use of resistors in an equivalent

Table 3. Comparison between three cases of MIMO antenna

Antenna type	Bandwidth (GHz)	Isolation (dB)	Max. ECC
Both AE1	3–11 (−11.7 dB)	>23.2	0.043
Both AE2	3–10.9 (−11.5 dB)	>21.5	0.050
AE1 + AE2 (Proposed)	3–11 (−12.2 dB) (AE1) 3–10.8 (−11.3 dB) (AE2)	>30.7	0.004

https://doi.org/10.1017/S1759078722000757 Published online by Cambridge University Press

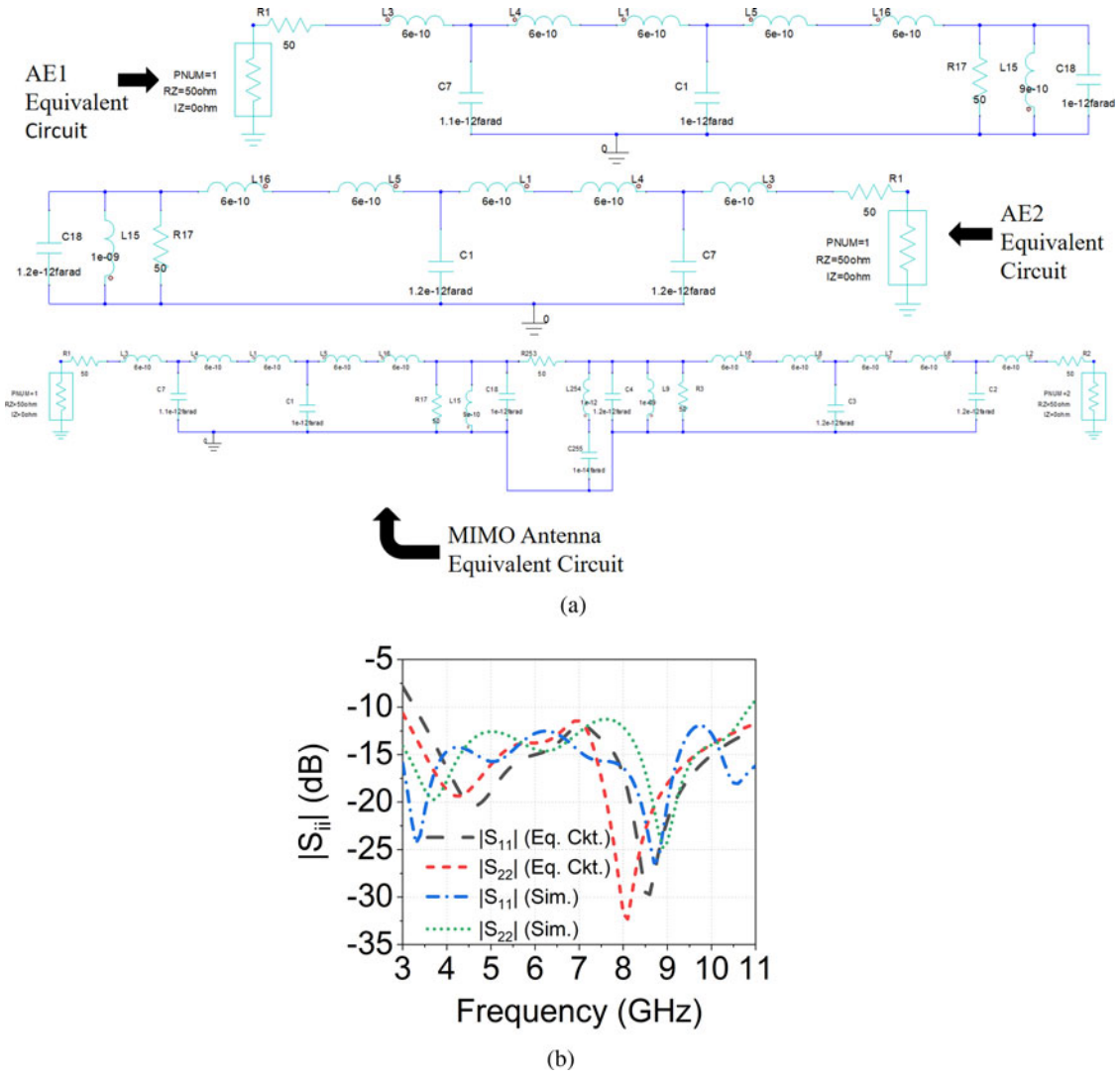


Fig. 4. (a) Equivalent circuit diagram of AEs and MIMO antenna and (b) S_{ii} of equivalent circuit and simulated MIMO antenna.

circuit and also both ports are fed with a lossy transmission line, which is implemented with a resistively loaded microstrip line [28]. As shown in Fig. 4(a) all microwave ports are terminated with a 50 Ω load impedance and all other resistors are equal to 50 Ω. The structure of step discontinuity is modeled as a T-structure containing two inductors and a capacitor. The 10 mm gap can be modeled as a group of R-L-C, which is placed in the middle of AE circuits. The starting values of the resistors, capacitors, and inductors are obtained from the references [29, 30] and to obtain the desired bandwidth, these values are optimized. The equivalent circuit reflection coefficients are almost identical to simulated reflection coefficients as shown in Fig. 4(b).

Characteristic modes (CM) analysis

The CM analysis is carried out using an integral equation solver of CST Studio Suite. The antenna structure should be a perfect electric conductor (PEC) with 0 mm height on account of the impediments of the integral equation solver and the layer of the substrate should be eliminated for the benefit of MoM computing. The characteristic angle (CA) is used to check whether the PEC structure radiates efficiently or not and modal significance (MS) is used to evaluate the contribution of each mode in the total electromagnetic. Both can be measured using the following expressions [31]

$$MS = \left|\frac{1}{1 + j\lambda_n}\right| \tag{5}$$

$$CA = 180^{\circ} - tan^{-1}\lambda_n \tag{6}$$

where λ_n is the Eigen values, and n is the order index of each mode.

The predicted CAs of the presented AE 1 and AE 2 are presented in Figs 5(a) and 5(b), respectively. The four CM of the AE1 resonates at 6.7, 7.6, 3.7 and 8.7 GHz, while the four CM

https://doi.org/10.1017/S1759078722000757 Published online by Cambridge University Press

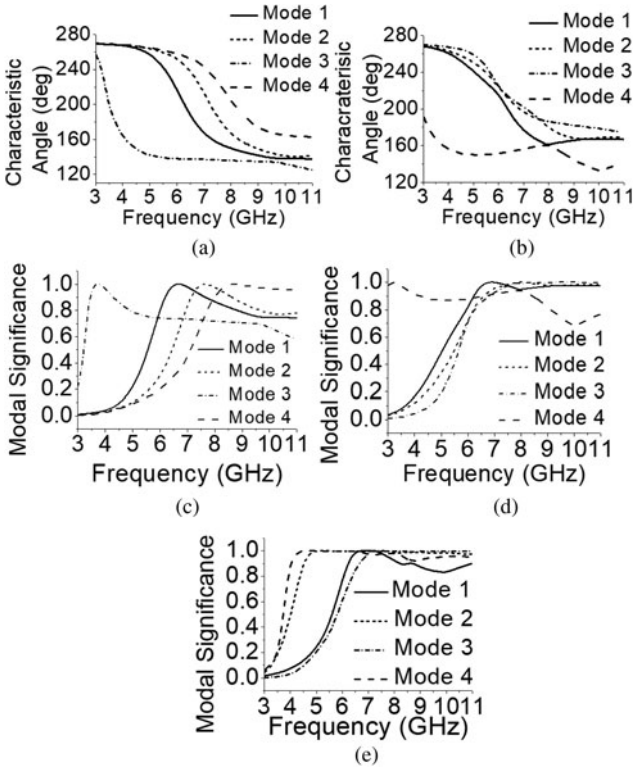


Fig. 5. (a) Characteristic angles of AE 1, (b) Characteristic angles of AE 2, (c) Modal significances of AE 1 (d) Modal significance of AE 2, and (e) Modal significance of MIMO antenna.

of the AE2 resonate at 6.9, 8, 9.7 and 3.2 GHz. The equivalent modal significances (MSs) of the four CM of the AE 1 and AE 2 are displayed in Figs 5(c) and 5(d), which shows that the MSs curves of AE 1 are sharper than AE 2, therefore, the four CM of AE 1 have narrower bandwidth than AE 2. This fact can be clarified by seeing their quality (Q) factors. AE 1 has high Q-factors than AE 2 resulting in narrower bandwidth [32]. The bandwidth of AE 2 (3 to 10.3 GHz) is larger than AE 1 (3 to 9.5 GHz) when simulated separately (Fig. 2(c)). With a high Q-factor, impedance matching of a small electrical size antenna gets deteriorated, when its impedance bandwidth, resonance frequency, and radiation efficiency are constant [32]. The current distribution of all modes of the AE 1 and AE 2 is shown in Fig. 6. In AE1, the main current of Mode 1 has the same orientation in the feeding line and tapered patch. In Mode 2, the main current inverts its orientation at the ground taper. The main current of Mode 3 has the same orientation in the ground taper, and the current flows from right to left in the rectangular ground (connected to the taper). In Mode 4, the main current reverses its direction at the feeding point and after starting the taper. In AE2, the main current of Mode 1 flows in the loop (anti-clockwise) in the circular monopole patch, and single direction on the ground from right to left. The main currents of Mode 2 have an upward direction and the main direction of Mode 4 has a downward direction. In Mode 3, the main current flows in an anti-clockwise direction in the ground surface and circular monopole.

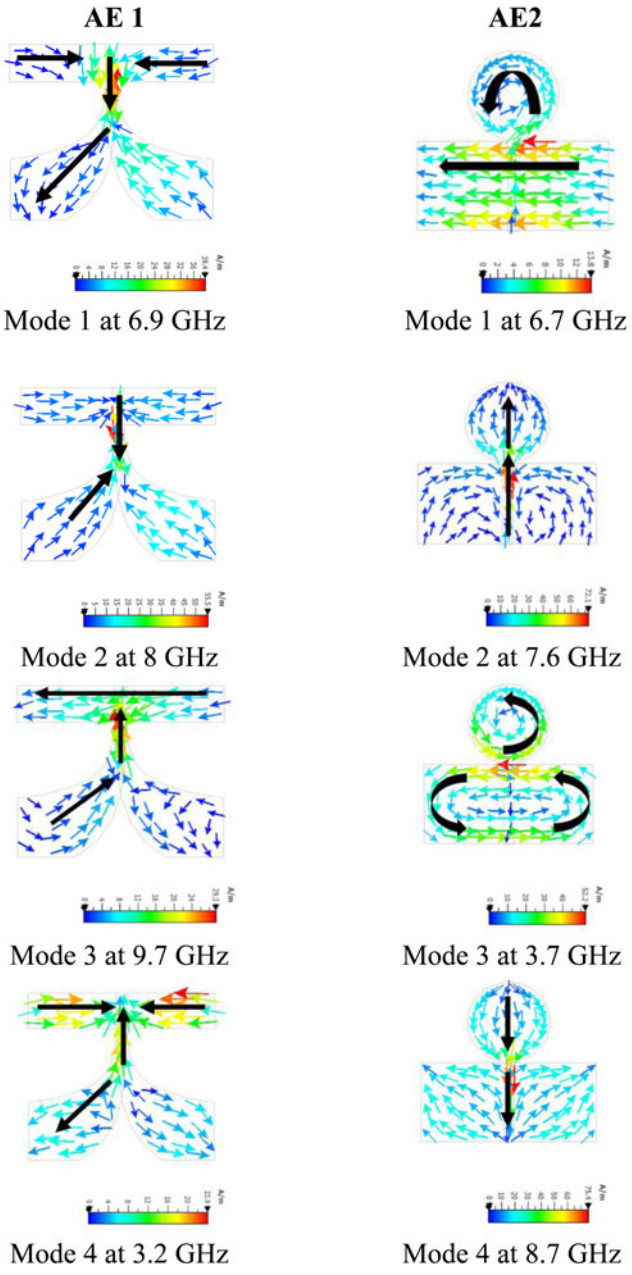


Fig. 6. The current distribution of all modes of AE 1 and AE 2.

CM analysis of presented antenna

To disclose the process of obtaining the distinctive radiation patterns in the designed antenna, the connection between the AEs and the ground plane is investigated. For instance, the most significant CMs of both AE1 and AE2 are chosen, which are excited around 6.8 GHz as presented in Figs 5(a) and 5(b). Thus, CM analysis emphasizes 6.8 GHz. The MSs of the antenna's ground surface of the MIMO antenna are portrayed in Fig. 5(e), which indicates that Mode 1 and Mode 3 of the ground surface are excited around 6.8 GHz.

Figure 7 shows the electric fields, magnetic fields, surface current distributions, and far-field patterns of the antenna's

https://doi.org/10.1017/S1759078722000757 Published online by Cambridge University Press

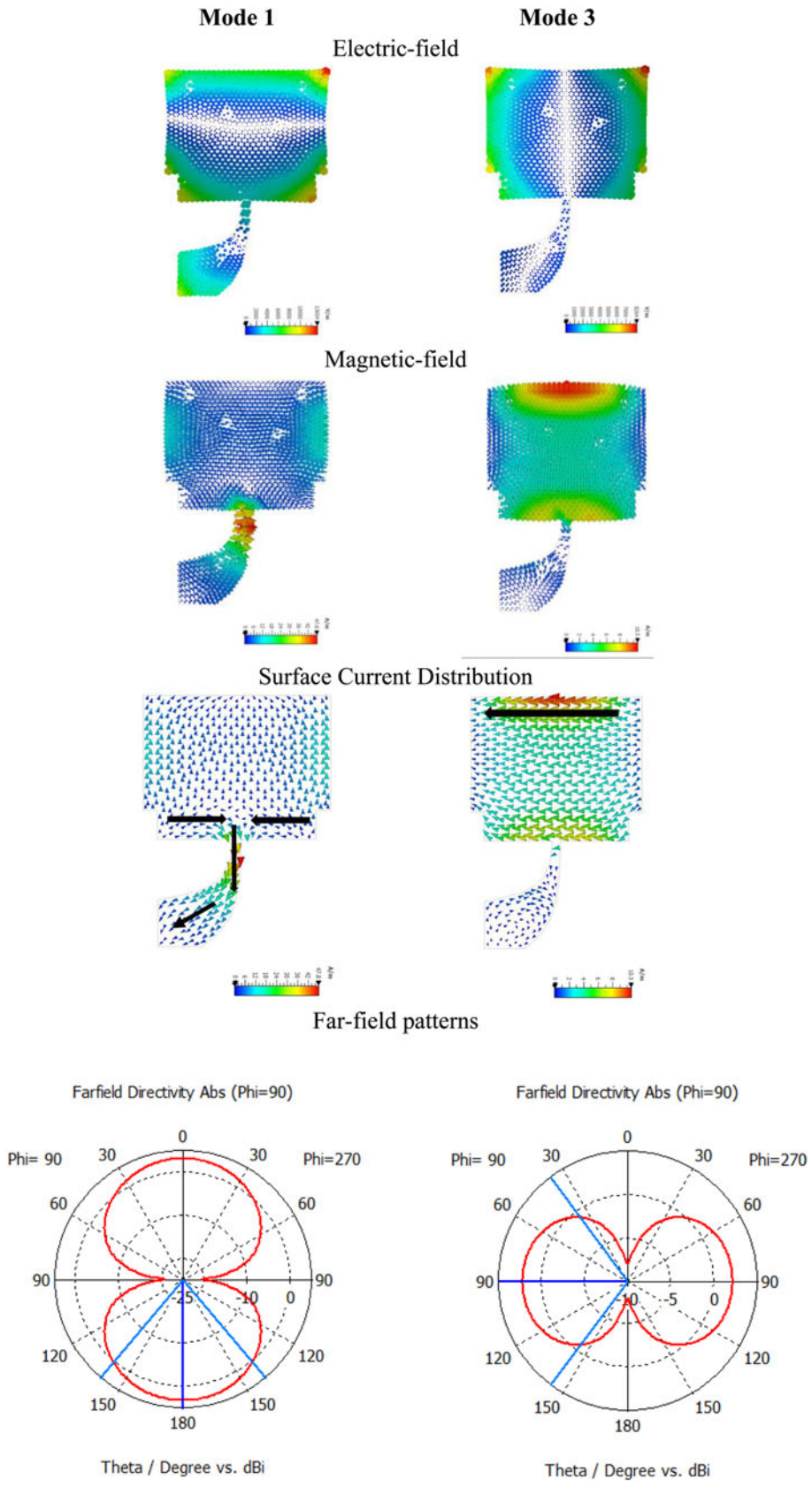


Fig. 7. Predicted electric fields, magnetic fields, surface current distribution, and far-field patterns of the antenna's ground surface at 6.8 GHz of Mode 1 and Mode 3.

https://doi.org/10.1017/S1759078722000757 Published online by Cambridge University Press

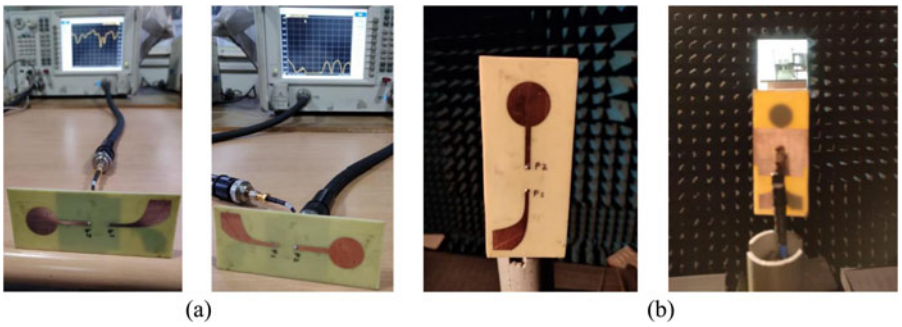


Fig. 8. Measurement setup (a) VNA setup for S_{11} and S_{21} measurement, (b) Anechoic chamber setup for radiation pattern measurement.

ground surface at 6.8 GHz. Mode 1 has strong electric fields and nulls of magnetic fields and Mode 3 has nulls of electric fields and strong magnetic-field around the place of AEs (Fig. 7). As displayed in surface current distribution, there is strong current distribution around AE1 in Mode 1 and AE2 in Mode 3. Consequently, AE1 excites Mode1 and AE2 excites the Mode3 of the ground surface. Furthermore as displayed in Fig. 5, the radial current exuding from AE1 at 6.9 GHz infers that AE1 acts as an electric source, which implies that the AE mainly stores electric energy. When an electric source is appropriately located at the strong electric-field location of a CM, it excites the CM successfully [22]. Thus, AE1 can excite Mode1 of the ground surface successfully. Interestingly, the current of AE2 structures a loop at 6.7 GHz. On such an occasion, AE2 refer to as a magnetic source, which implies that the AE mainly stores magnetic energy. When a magnetic source is appropriately located at the strong magnetic-field location of a CM, it can energize the CM efficiently [22]. In like manner, AE2 excites Mode 3 of the ground surface successfully. The far-field radiation patterns of Mode 1 and Mode 3 of the ground surface are introduced in Fig. 7. The bidirectional pattern of Mode 1 has its greatest radiation along the 180° direction, while the bidirectional pattern of Mode 3 has its most extreme radiation along the 90° direction. The two radiation patterns have practically a similar shape with orthogonal direction. It is derived from this that the two patterns are orthogonal to one another.

Results and discussion

The measurement of s-parameters of the presented antenna is tested using Vector Network Analyser and the measurement of far-field patterns is done in an anechoic chamber as displayed in Fig. 8.

Both simulated and measured results are almost identical. The measured operating bandwidth of AE1 is from 2.57 GHz to >20 GHz as illustrated in Fig. 9(a) with measured peak gain from 0.83 to 6.4 dB within the bandwidth of 3 to 20 GHz. The experimental operating bandwidth of AE2 is from 2.23 GHz to 11.09 GHz with a slight mismatch around 7.5 GHz and the measured peak gain of AE2 is from 0.86 dB to 6 dB within the bandwidth 3 to 20 GHz as presented in Fig. 9(b). The reasons for the slight variations in simulated and experimental s-parameters and gain are fabrication tolerance, material loss, and connector loss. The presented MIMO antenna has isolation>30.1 dB with a bandwidth from 2.82 GHz to 14.5 GHz, as presented in Fig. 9(c). The presented antenna shows radiation efficiency of over 75% in the UWB range, as demonstrated in Fig. 9(d). The envelope correlation coefficient (ECC) is the essential factor to predict the MIMO/diversity performance. It determines how much the radiation patterns of AEs are differing. The ECC is <0.08 from 1.54 GHz to >20 GHz as presented in Fig. 9(e), which is calculated using *S*-parameters [7].

$$ECC = \frac{\left|\iint [\vec{F_i}(\theta, \phi)] d\Omega\right|^2}{\iint |\vec{F_i}(\theta, \phi)|^2 d\Omega . \iint |\vec{F_j}(\theta, \phi)|^2 d\Omega} \quad (7)$$

where $\vec{F_i}$ and $\vec{F_j}$ are the *i*th and *j*th antenna radiated fields.

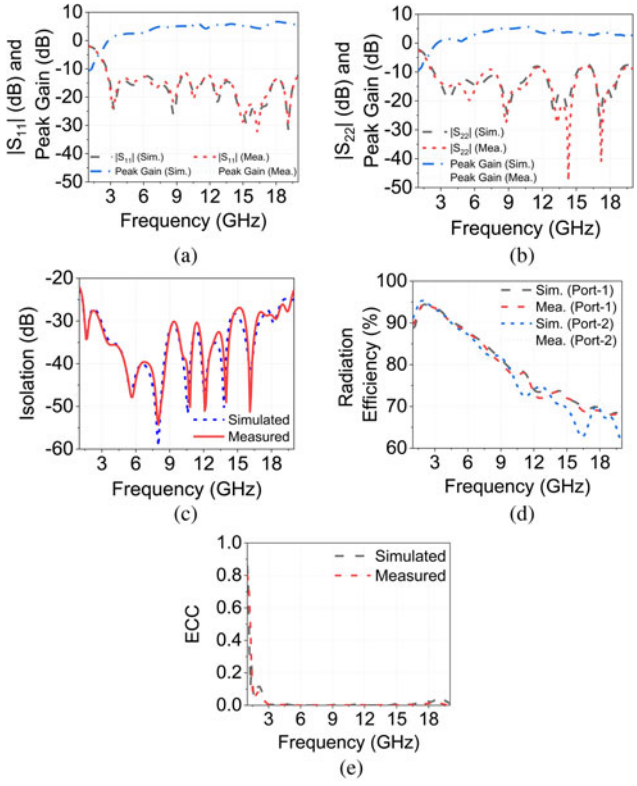


Fig. 9. MIMO Antenna results: (a) *S*-parameters and peak gain of AE1, (b) S-parameters and peak gain of AE2, (c) Isolation between AE1 and AE2, (d) Radiation efficiency, and (e) ECC.

https://doi.org/10.1017/S1759078722000757 Published online by Cambridge University Press

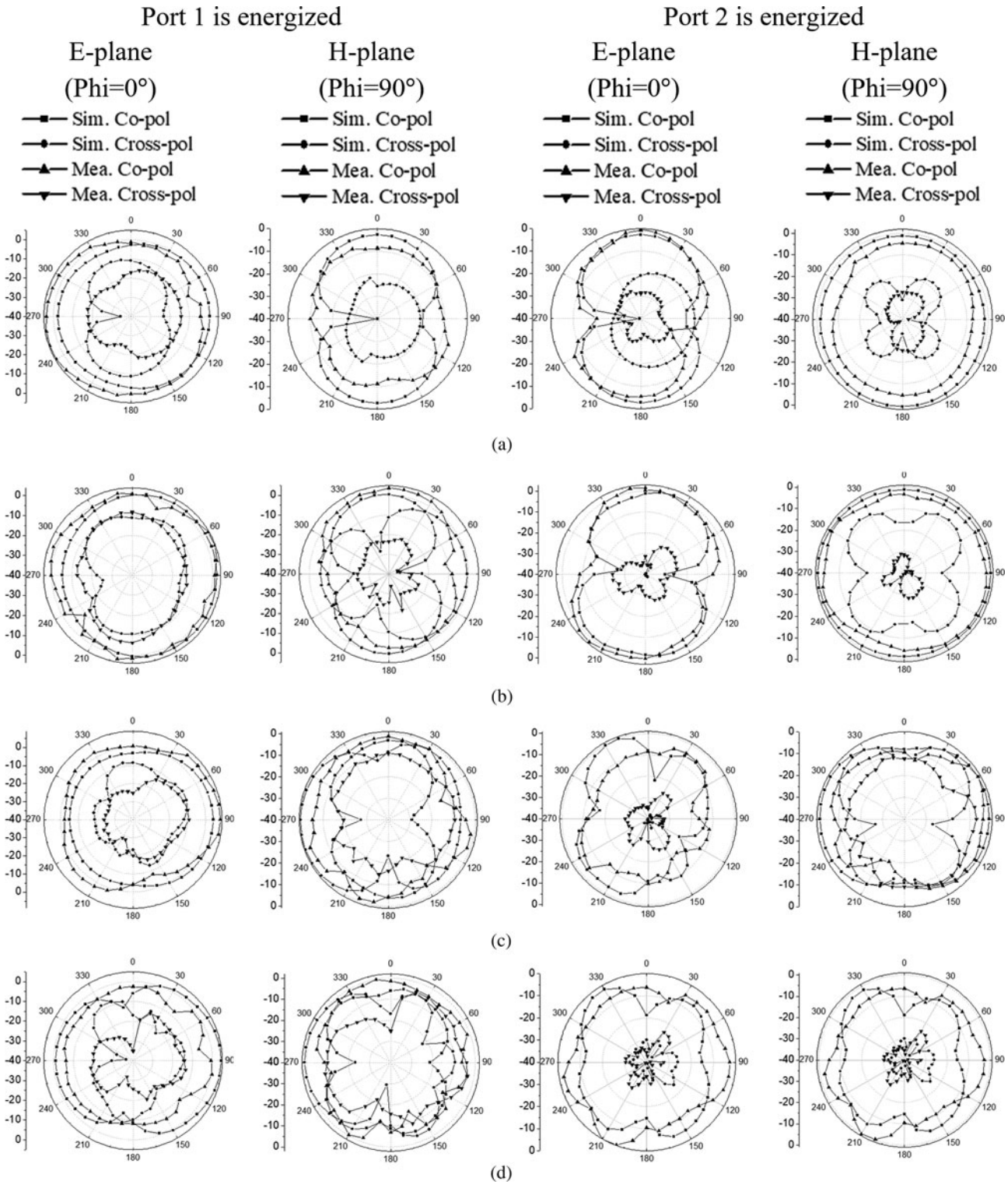


Fig. 10. Radiation patterns when Port1 and Port 2 are energized at (a) 3 GHz,(b) 5 GHz,(c) 7 GHz, and (d) 9 GHz.

As shown in Fig. 10, when port 1 is energized, an almost omnidirectional shape radiation pattern is attained in E-plane, and a bidirectional shape radiation pattern is achieved in H-plane. However, when port 2 is excited, a bidirectional shape radiation pattern is obtained in E-plane and an almost omnidirectional shape radiation pattern in H-plane. Because of this swapping of the shape of the radiation patterns, high isolation is obtained and very low ECC is achieved. As shown in

https://doi.org/10.1017/S1759078722000757 Published online by Cambridge University Press

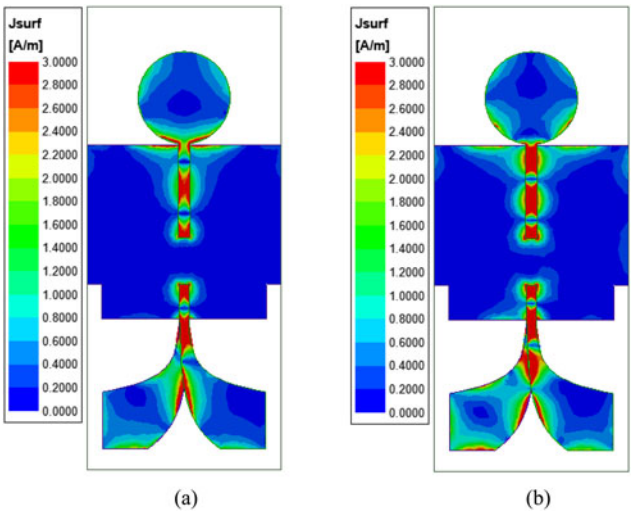


Fig. 11. Surface current distribution at (a) 7 GHz and (b) 9 GHz.

Fig. 11, 7 GHz indicates approximately a second-order harmonic, and a more complex current pattern is generated at 9 GHz, as compared to the third-order harmonic. Therefore, because of the generation of higher-order modes at higher frequencies, cross-polarization increases. The maximum acceptable limit of cross-polarization is −15 dB for practical purposes. The cross-polarized patterns in H-plane are almost comparable to the acceptable limits.

In Table 4, the performance of the proposed antenna is compared with recently reported UWB MIMO antennas with two AEs. The highest isolation is obtained by the proposed antenna using excitation of different modes in the ground surface shared by antipodal Vivaldi and circular monopole AEs as compared to other recently reported antennas. In reference [30], the same concept of exciting different CM in the ground surface is used for pattern diversity and isolation increment. However, this antenna is not applicable for UWB applications because complete UWB bandwidth is not achieved by both AEs. Also, the isolation of this antenna is lower than the presented antenna.

Conclusion

A printed UWB MIMO antenna with improved isolation and distinct (far-field) patterns is designed, which is explained using CM. The designed dual AEs stimulate different CM over the working frequency band, therefore obtaining high isolation without DS requirement and distinct far-field radiation patterns. The measured results verify that both AEs work from 2.6 GHz to 11 GHz. The isolation is >30.1 dB in UWB. The peak realized gain is more than 0.83 dBi. The radiation efficiency is above 75%. The ECC is below 0.08. The presented antenna has an appropriate design for emerging mobile terminals.

Table 4. Comparison between the presented antenna and other two-port UWB MIMO antennas.

Ref.	Bandwidth (GHz)	Isolation (dB)	Peak Gain (dB)	ECC	Method	Antenna organization
[8]	2.26–20	>20.6	4.8	0.001	Without DT	Orthogonal
[9]	1.7–14	>20.2	0.4–4.8	0.09	DS	180° Rotation
[10]	3.1–10.6	>20	Not Mentioned	0.003	Without DT	180° Rotation
[7]	2.95–15.65	>25	1.2–6.8	0.04	Parasitic Elements	Parallel
[11]	3.06–13.41	>17.07	2–6	0.05	DS	Parallel
[12]	1.83–13.82	>21	4–7.48	0.039	DS	Parallel
[13]	4–10	>20	0–4	0.016	DS	Parallel
[14]	2.44–10.64	>15	Not Mentioned	Not Mentioned	DS	Parallel
[15]	3–13	>15	7	0.5	DS	Parallel
[17]	2–20	>25	0–7	0.05	DGS	Parallel
[18]	3.9–11.5	>15	Not Mentioned	0.04	DGS	Parallel
[19]	3.2–12	>16	Not Mentioned	Not Mentioned	Metamaterial Frequency Selective Surface (FSS)	Parallel
[20]	3.5–11	>22	2.91	0.084	Neutralization Line	Parallel
[21]	2.5–11	>15	4.6	0.01	Carbon Black Film	Parallel
[25]	2–9.5 (both AEs)	>20	6	0.03	Different CM	Opposite edges
This work	**2.6–11 (both AEs)**	**>30.1 (in UWB)**	**6.4 (AE1), 6 (AE2)**	**0.08**	**Different CM**	**Opposite edges**

https://doi.org/10.1017/S1759078722000757 Published online by Cambridge University Press

References

1. **Chin WH, Fan Z and Haines R** (2014) Emerging technologies and research challenges for 5 G wireless networks. *IEEE Wireless Communications* **21**, 106–112.
2. **Gupta A and Jha RK** (2015) A survey of 5 G network: architecture and emerging technologies. *IEEE Access* **3**, 1206–1232.
3. **Shafi Mansoor, Molisch Andreas F., Smith Peter J., Haustein Thomas, Zhu Peiying, Silva Prasan De, Tufvesson Fredrik, Benjebbour Anass and Wunder Grehard** (2017) 5 G: a tutorial overview of standards, trials, challenges, deployment, and practice. *IEEE Journal on Selected Areas in Communications* **35**, 1201–1221.
4. **Antenna Diversity, Wikipedia, May 2018. [Online]**. Available at https://en.wikipedia.org/wiki/Antenna_diversity.
5. **Antenna Diversity Basics, RF Wireless World, [Online]**. Available at https://www.rfwireless-world.com/Articles/Antenna-diversity-basics-and-diversity-types.html.
6. **Choudhary S, Jha S and Sharma P** (2014) A Review of Diversity Techniques in Wireless Communication system. in *Proceedings of National Conference on Recent Advances in Electronics and Communication Engineering*.
7. **Addepalli T and Anitha VR** (2020) Compact Two-port MIMO antenna with high isolation using parasitic reflectors for UWB, X and Ku band applications. *Progress In Electromagnetic Research C* **102**, 63–77.
8. **Jayant S, Srivastava G and Purwar R** (2021) Bending and SAR analysis on UWB wearable MIMO antenna for on-arm WBAN applications. *Frequenz* **75**, 177–189.
9. **Wang M, Nan J and Liu J** (2021) High-isolation UWB MIMO antenna with multiple X-shaped stubs loaded between ground plane. *International Journal of Antennas and Propagation* **2021**, 1–13.
10. **Wu Y, Ding K, Zhang B, Li J, Wu D and Wang K** (2018) Design of a compact UWB MIMO antenna without decoupling structure. *International Journal of Antennas and Propagation* **2018**, 1–7.
11. **Gurjar R, Upadhyay DK, Kanaujia BK and Kumar A** (2021) A compact U-shaped UWB-MIMO antenna with novel complementary modified Minkowski fractal for isolation enhancement. *Progress In Electromagnetics Research C* **107**, 81–96.
12. **Dey AB, Pattanayak SS, Mitra D and Arif W** (2020) Investigation and design of enhanced decoupled UWB MIMO antenna for wearable applications. *Microwave and Optical Technology Letters* **63**, 845–861.
13. **Abdelraheem A and Abdalla MA** (2018) Bi-directional UWB MIMO antenna for superior spatial diversity, and/or multiplexing MIMO performance. *Wireless Personal Communications* **101**, 1379–1394.
14. **Kim S and Choi J** (2018) Two-Port UWB MIMO Antenna with Modified Ground for Isolation Improvement. in *2018 International Symposium on Antennas and Propagation (ISAP)*, Busan, Korea.
15. **Mamilla N** (2019) CPW Feed flag shaped array antenna on common ground for UWB MIMO and IOT applications. *International Journal of Innovative Technology and Exploring Engineering (IJITEE)* **8**, 1337–1342.
16. **Bhattacharjee A, Karmakar A, Saha A and Bhattacharya D** (2021) Design of a compact UWB MIMO-diversity antenna incorporating fractal inspired isolation structure with band notch characteristics. *Microwave and Optical Technology Letters* **63**, 2597–2605.
17. **Sharma MK, Kumar M and Saini JP** (2021) Design and analysis of a compact UWB-MIMO antenna with improved isolation for UWB/WLAN applications. *Wireless Personal Communications* **119**, 2913–2928.
18. **Jansari DV and Amineh RK** (2019) A two-element antenna array for compact portable MIMO-UWB communication systems. *AIMS Electronics and Electrical Engineering* **3**, 224–232.
19. **Zhu X, Yang X, Song Q and Lui B** (2017) Compact UWB-MIMO antenna with metamaterial FSS decoupling structure. *Wireless Personal Communications* **115**, 2–6.
20. **Tiwari RN, Singh P, Kanaujia BK and Srivastava K** (2019) Neutralization technique based two and four port high isolation MIMO antennas for UWB communication. *International Journal of Electronics and Communications* **110**, 1–10.
21. **Lin G, Sung C, Chen J, Chen L and Houng M** (2017) Isolation improvement in UWB MIMO antenna system using carbon black film. *IEEE Antennas and Wireless Propagation Letters* **16**, 222–225.
22. **Li H, Lau BK, Ying Z and He S** (2012) Decoupling of multiple antennas in terminals with chassis excitation using polarization diversity, angle diversity and current control. *IEEE Transactions on Antennas and Propagation* **60**, 5947–5957.
23. **Szini I, Tatomirescu A and Pedersen GF** (2015) On small terminal MIMO antennas, harmonizing characteristic modes With ground plane geometry. *IEEE Transactions on Antennas and Propagation* **63**, 1487–1497.
24. **Bouezzeddine M and Schroeder WL** (2016) Design of a wideband, tunable four-port MIMO antenna system With high isolation based on the theory of characteristic modes. *IEEE Transactions on Antennas and Propagation* **64**, 2679–2688.
25. **Zhao X, Yeo SP and Ong LC** (2018) Planar UWB MIMO antenna With pattern diversity and isolation improvement for Mobile platform based on the theory of characteristic modes. *IEEE Transactions on Antennas and Propagation* **66**, 420–425.
26. **Hood AZ, Karacolak T and Topsakal E** (2008) A small antipodal Vivaldi antenna for ultrawide-band applications. *IEEE Antennas and Wireless Propagation Letters* **7**, 656–660.
27. **Thomas KG and Sreenivasan M** (2010) Simple ultrawideband planar rectangular printed antenna with band dispensation. *IEEE Transactions on Antennas and Propagation* **58**, 27–34.
28. **Pfeiffer C, Steffen T and Kakas G** (2019) Lossy Antenna Arrays with Frequency-Independent Beamwidth. in *IEEE International Symposium on Antennas and Propagation and USNC-URSI Radio Science Meeting*, Atlanta, GA, USA.
29. **Kasi B, Jalil YE and Chakrabarty CK** (2013) Circuit Modeling for UWB-MIMO Antenna Array. in *2013 IEEE International RF and Microwave Conference*, Penang, Malaysia.
30. **Jangid S and Kumar M** (2013) An equivalent circuit of UWB patch antenna with band notched characteristics. *International Journal of Engineering and Technology* **3**, 159–164.
31. **Liu Jun Feng, Tang Wenxuan, Wang Meng, Zhang Hao Chi, Ma Hui Feng, Fu Xiaojian and Cui Tie Jun** (2020) A dual-mode UWB antenna for pattern diversity application. *IEEE Transactions on Antennas and Propagation* **68**, 3219–3224.
32. **Hansen RC and Collin RE** (2011) *Small Antenna Handbook*. Hoboken, NJ, USA: John Wiley & Sons.



Shailesh Jayant received the B.Tech. degree in electronics and communication engineering from Bhagwan Parshuram Institute of Technology, which is affiliated with Guru Gobind Singh Indraprastha University (GGSIPU), Delhi-110089, India in 2014, and an M.Tech, degree in microwave electronics from the Department of Electronic Science, University of Delhi, South Campus, New Delhi- 110021, India, in 2017. She is currently pursuing a Ph.D. degree in electronics and communication engineering from Ambedkar Institute of Advanced Communication Technologies and Research, Delhi–110031, India (also affiliated to GGSIPU), Delhi- 110078, India). She has published six journal papers and three IEEE conference papers. Her current research interests include the design of UWB MIMO antenna, microwave filters, and broadband power amplifiers.



Garima Srivastava is presently working as an assistant professor in the Department of Electronics & Communication Engineering at Netaji Subhas University of Technology (Formerly Ambedkar Institute of Advanced Communication Technologies & Research), Geeta Colony, Delhi. She had joined this institute in 2011, through selection by Union Public Service Commission. She holds her Ph.D. in electronics and communication engineering in the area of RF and microwave and she received her master's degree in electronics from Allahabad University, India. She has a keen interest in the microstrip antenna,

https://doi.org/10.1017/S1759078722000757 Published online by Cambridge University Press

UWB antenna, reconfigurable, and circularly polarized antenna, wireless communication, and MIMO technologies. She has more than 35 published papers in refereed National/International Journals & Conferences.



Sachin Kumar received the B.Tech. degree from Uttar Pradesh Technical University, Lucknow, India, in 2009, and the M.Tech. and Ph.D. degrees from Guru Gobind Singh Indraprastha University, Delhi, India, in 2011 and 2016, respectively. He was a post-doctoral research fellow at the College of IT Engineering, Kyungpook National University, South Korea, from 2018 to 2021. He is currently working as a research assistant professor with the Department of Electronics and Communication Engineering, SRM Institute of Science and Technology, Chennai, India. Dr. Kumar has published 04 patents, 02 books, and more than 120 research articles in several peer-reviewed international journals and conferences. He serves as an Advisory Board Member for the Journal *Measurement*, Editorial Board Member for the Journal *Current Chinese Science*, and Guest Editor for the *International Journal of Antennas and Propagation*. He is also a frequent reviewer for more than 60 scientific journals and book publishers. He serves as the session chair, organizer, and member of the technical program committee for various international conferences, summits, and workshops. He was a recipient of the Teaching-cum-Research Fellowship from the Government of NCT of Delhi, India, and the Brain Korea 21 Plus Research Fellowship from the National Research Foundation of South Korea. He is a Life Member of the Indian Society for Technical Education and the Korean Institute of Electromagnetic Engineering and Science.

https://doi.org/10.1017/S1759078722000757 Published online by Cambridge University Press